THE JOURNAL OF PHYSICAL CHEMISTRY LETTERS
A JOURNAL OF THE AMERICAN CHEMICAL SOCIETY

pubs.acs.org/JPCL

Letter

Dielectric Screening Modulates Semiconductor Nanoplatelet Excitons

Ashley J. Shin, Azmain A. Hossain, Stephanie M. Tenney, Xuanheng Tan, Lauren A. Tan, Jonathan J. Foley IV, Timothy L. Atallah,* and Justin R. Caram*

Cite This: J. Phys. Chem. Lett. 2021, 12, 4958–4964

Read Online

ACCESS | Metrics & More | Article Recommendations | Supporting Information

ABSTRACT: The influence of external dielectric environments is well understood for 2D semiconductor materials but overlooked for colloidally grown II–VI nanoplatelets (NPLs). In this work, we synthesize MX (M = Cd, Hg; X = Se, Te) NPLs of varying thicknesses and apply the Elliott model to extract exciton binding energies—reporting values in good agreement with prior methods and extending to less studied cadmium telluride and mercury chalcogenide NPLs. We find that the exciton binding energy is modulated both by the relative effect of internal vs external dielectric and by the thickness of the semiconductor material. An analytical model shows dielectric screening increases the exciton binding energy relative to the bulk by distorting the Coulombic potential across the NPL surface. We further confirm this effect by decreasing and recovering the exciton binding energy of HgTe NPLs through washing in polarizable solvents. Our results illustrate NPLs are colloidal analogues of van der Waals 2D semiconductors and point to surface modification as an approach to control photophysics and device properties.

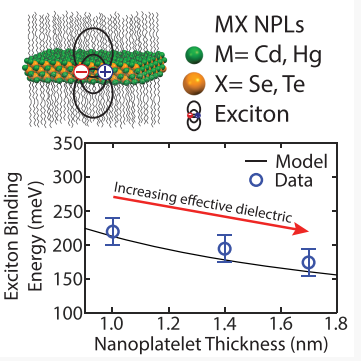

Colloidal nanoplatelets (NPLs) are an emerging class of optoelectronic substrates, useful due to their high absorptivities, near unity quantum yields, and narrow tunable quantum confined emission.[1−4] Another appealing aspect of these NPLs is the atomic precision over their growth anisotropy: II–VI cadmium chalcogenide NPLs can be synthesized with precisely 2–11 monolayer (ML) thicknesses and show increasing control over their 2D lateral extent.[5−9] Such structures can also template other II–VI NPLs, including core–shell and core–crown Cd/Zn S/Se/Te heterostructures and mercury chalcogenide infrared emitters, which demonstrate comparable synthetic control.[10−12] With increased tunability of the NPL thickness, colloidal 2D materials warrant further exploration of the extent of synthetic modulation over their photophysical properties and device applicability. In this work, we measure the absorption spectra of zinc-blende II–VI NPLs, which consist of alternating M–X atomic layers (M = Cd, Hg and X = Se, Te), as shown in Figure 1a. The NPLs have thicknesses of 0.7–1.9 nm and lateral dimensions of 50–200 nm (Figure 1b).[13−15] The synthesis procedures for individual NPLs and material characterization can be found in the Supporting Information (Supporting Information Sections I and II; EDS in Table S1, FTIR in Figures S1 and S2, and TEM in Figures S3 and S4). Motivated by their similarity to other 2D excitonic semiconductors, such as quantum wells and transition metal dichalcogenides (TMDCs), we use the distinct room temperature features of the absorption spectra (Figure 1c) to understand bandgap and excitonic properties. In this work, we apply the Elliott model to fit excitonic absorption features.[16−19] We extract light and heavy hole exciton binding energies (E_B) that are in excellent agreement with the prior limited available experimental results for the heavy hole exciton binding energy in CdSe NPLs.[20,21] In all NPLs, we observe high exciton binding relative to the case for bulk semiconductors.

In layered van der Waals semiconductors, high binding energies are attributed to the strong influence of the external dielectric on E_B.[22] To test whether external dielectric plays a similar role in 2D NPLs, we study the thickness and solvent dependence on exciton binding energy. We observe that as the NPL thickness increases, the exciton binding energy decreases, a result that we can recover quantitatively through a minimal electrostatic model of variable thickness dielectric slabs. We further demonstrate dielectric modulation of binding energy by shifting and recovering HgTe E_B through exchange in polarizable solvent. Our results expand upon established colloidal NPLs' excitonic properties and emphasize the importance of the dielectric environment in modulating the photophysical properties.

To establish factors influencing colloidal NPL excitons, we use the absorbance spectra to derive photophysical constants, such as exciton binding energy and band-to-band energy

Received: February 25, 2021
Accepted: May 13, 2021
Published: May 19, 2021

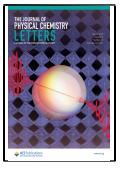

https://doi.org/10.1021/acs.jpclett.1c00624
J. Phys. Chem. Lett. 2021, 12, 4958–4964

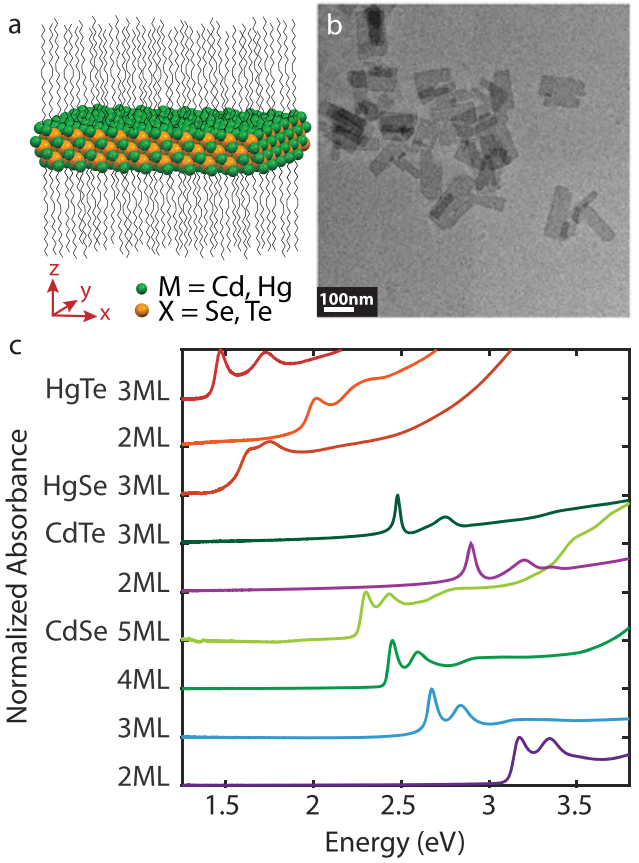

Figure 1. (a) Simplified crystal structure of 3 ML MX (M = Cd, Hg; X= Se, Te) NPL, including organic ligands as an example. (b) TEM image of 3 ML HgSe NPLs, showing nanoscale lateral dimensions. (c) Normalized absorbance spectra of MX NPLs of varying thicknesses, offset for clarity.

difference (bandgap, E_G), through Elliott model fits. This straightforward method allows for high-throughput measurements to determine E_B values as well as easily monitoring solvent dielectric effects on E_B.

Multiband Elliott Model of Colloidal NPL Systems. The Elliott model describes absorption spectra of 2D and 3D semiconductors, accounting for excitonic resonances and oscillator strengths. The model yields optical transitions, corresponding to excitations from the ground state (valence band electrons) to bound electron−hole excitonic states, followed by a higher energy valence-band to conduction-band continuum of free electron transitions. The absorption features depend on the dimensionality of the semiconductor as shown in eq 1:

$$\alpha_D(E) \propto \sum_{n=1}^{\infty} \left(\frac{E_B \Gamma(n + D - 2)}{(n-1)!\left(n + \frac{D-3}{2}\right)^{D+1}} \cdot \delta\left(E - E_G + \frac{E_B}{\left(n + \frac{D-3}{2}\right)^2}\right) \right) + \frac{\left|\Gamma\left(\frac{D-1}{2} + i\beta\right)\right|^2 e^{\pi\beta} \beta^{2-D}}{2^D \pi^{2-D/2} \Gamma\left(\frac{D}{2}\right)} \cdot \Theta(E - E_G) \quad (1)$$

where ω is the excitation frequency, D is the dimensionality of the model system, n is the number of discrete excitonic peaks, E_G is the bandgap energy, $\beta = \sqrt{\frac{E_B}{\hbar\omega - E_G}}$, $\Gamma(n) = (n-1)!$ is the gamma function, $\delta(a-b)$ is the Dirac delta function, and Θ is the Heaviside step function.[19−23] The model reproduces the intensity and absolute positions of absorption features using only E_B and E_G as inputs, for a given dimensionality constant D. The Elliott model has been used to describe interband transitions in TMDCs, quantum wells, and 2D layered perovskites but has not been applied to NPLs.[16,23−28]

In Figure 2a, we illustrate the electronic structure of II−VI NPLs and highlight the transitions that are well-described by

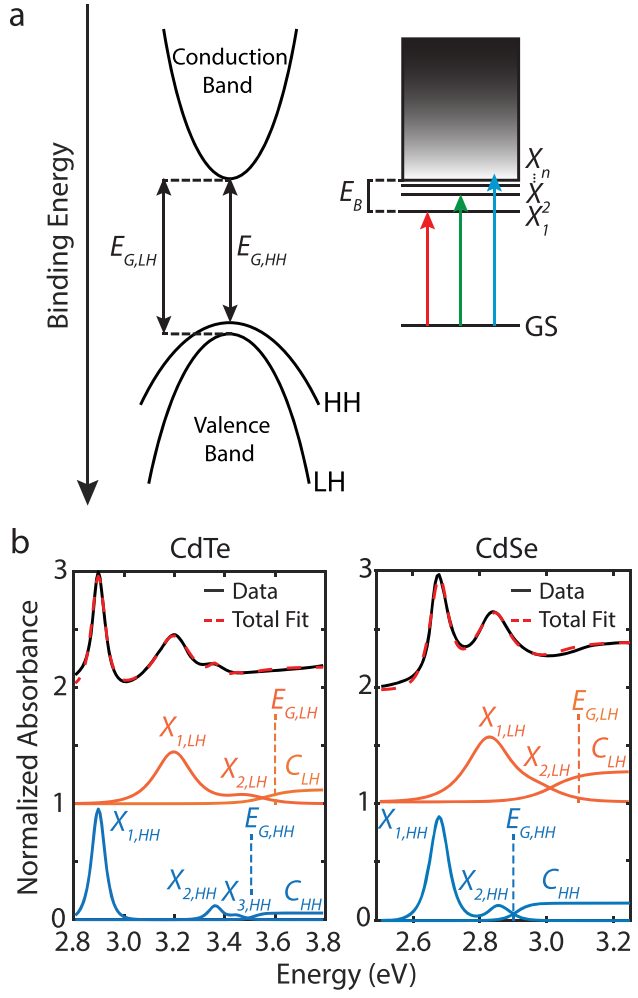

Figure 2. (a) Left: band diagram, showing both light hole (LH) and heavy hole (HH) valence bands. Right: general transition diagram for a HH or LH exciton. (b) Absorption spectra of 2 ML CdTe and 3 ML CdSe NPLs, showing the excitonic features of the modified Elliott model, offset for clarity. The X_n transitions and the onset of the conduction bands (C) are shown.

the Elliott model. The valence band is split into nondegenerate heavy hole (HH) and light hole (LH) bands, which are offset due to spin−orbit coupling.[29,30] In excitonic materials, the exciton binding energy is greater than thermal energy at room temperature ($E_B > kT$). This results in the observed excitonic transition peaks (Figure 2a: GS → X_n) within the absorption spectrum, appearing at lower energy than their corresponding

https://doi.org/10.1021/acs.jpclett.1c00624
J. Phys. Chem. Lett. 2021, 12, 4958−4964

Table 1. Bandgap and Exciton Binding Energies Extracted from Room-Temperature Absorption Data, Using a Modified Elliott Model[a]

NPL	MLs	$E_{G,HH}$ (eV)	$E_{B,HH}$ (meV)	$E_{G,LH}$ (eV)	$E_{B,LH}$ (meV)	bulk E_G (eV)/E_B (meV)
CdSe	2	3.5 ± 0.1	430 ± 30 220[j]	3.6 ± 0.1	220 ± 40	1.7[d]/15.7[e]
	3	2.91 ± 0.05	220 ± 20 210[b] 211 ± 5[I]/204[j]	3.1 ± 0.1	190 ± 30	
	4	2.65 ± 0.05	195 ± 20 190[b] 187 ± 2[I]/182[j]	2.7 ± 0.1	170 ± 30	
	5	2.45 ± 0.05	175 ± 20 170[b,c] 167 ± 2[I]/163[j]	2.5 ± 0.1	120 ± 30	
CdTe	2	3.51 ± 0.05	620 ± 30	3.6 ± 0.1	370 ± 35	1.54[f]/10.5[e]
	3	2.67 ± 0.05	210 ± 30	2.9 ± 0.1	200 ± 30	
HgSe	3	1.92 ± 0.05	300 ± 25	1.9 ± 0.1	190 ± 35	0[g]
HgTe	2	2.13 ± 0.05	450 ± 30	2.5 ± 0.1	300 ± 30	0[h]
	3	1.77 ± 0.05	350 ± 25	1.9 ± 0.1	260 ± 30	

[a]The CdX NPLs are passivatd by oleic acid ligands, whereas HgX NPLs are passivated by oleylamine. Both NPLs are suspended in hexanes. [b]Reference 20. [c]Reference 21. [d]Reference 33. [e]Reference 34. [f]Reference 35. [g]Reference 36. [h]Reference 37. [I]Semiempirical model. [j]Variational approach.

band-to-band continuum HH and LH transitions (Figure 2a: $E_{G,HH}$ and $E_{G,LH}$).

We extract the E_B and E_G values for the II−VI NPLs with various ML thicknesses by fitting our observed absorption spectra with the Elliott model (a more detailed explanation of the fitting procedure can be found in the Supporting Information Section III). To account for the line width broadening, we convolve eq 1 (where $D = 3$) with a tunable hyperbolic secant function $\left(\mathrm{sech}\left(\frac{\hbar\omega}{\gamma}\right)\right)$ resulting in the following expression:

$$\alpha_x(\omega) \propto \sum_{n=1}^{\infty} \frac{2E_B}{n^3}\,\mathrm{sech}\left(\frac{\hbar\omega - E_G + \frac{E_B}{n^2}}{\gamma}\right) + \int_{E_G}^{\infty} \mathrm{sech}\left(\frac{\hbar\omega - E'}{\gamma}\right)\frac{1}{1 - \exp\left(-2\pi\sqrt{\frac{E_B}{E' - E_G}}\right)}\,\mathrm{d}E' \tag{2}$$

where α_X is either α_{HH} or α_{LH}, γ is the line width broadening factor, and E' is the convolution integration energy variable (step-by-step process of the convolution in Supporting Information Section IV). We observe that the 3D Elliott model generates a better fit than 2D, which we hypothesize is the result of the finite thickness of NPLs. In Supporting Information Section V, we provide a mathematical and visual comparison between the two- and three-dimensional Elliott models and fits (Figure S5). We account for HH and LH absorption by fitting the sum $\alpha_{Total} = \alpha_{HH} + \alpha_{LH}$.[31,32] In Figure 2b, we show examples of typical NPL absorption spectra, the eq 2 fit, and fit components corresponding to HH and LH transitions. The spectra are broken down into contributions from continuum and excitonic features with labeled transitions. This straightforward application of the Elliott model determines the absolute positions of HH/LH excitonic transitions from the onset of the continuum. Thus, the modified Elliott model fits the absorption spectra using eight parameters—line-broadening as well as bandgap and exciton binding energies for light and heavy holes and amplitudes.

Bandgap and Exciton Binding Energies of CdX and HgX NPLs (X = Te, Se). The E_G and E_B values for the cadmium and mercury NPLs are shown in Table 1. We note reported values of binding energy in 3−5 ML CdSe NPLs, for which our measurement shows excellent agreement. As expected, the bandgap energy increases as the number of MLs decreases due to increasing quantum confinement. Furthermore, the exciton binding energy also increases as the number of MLs decreases. Interestingly, for the same number of MLs, HgX NPLs have higher E_B values (with the exception of 2 ML CdTe and HgTe), which is unexpected as mercury chalcogenides have larger dielectric constants than the cadmium ones.[38,39] This discrepancy may be explained by differences in surface lattice strain between 2 ML CdTe and HgTe, changing valence and conduction band structures, and electron−hole interactions.[40,41] Alternatively, our previous work suggests HgTe NPLs have their outer metal atomic layer stripped off during the cation exchange process, resulting in decreased charge density on the surface and a lower dielectric.[10] This would potentially result in a larger exciton binding energy in comparison to the metal terminated CdTe NPLs. In the next section we explore how layer number influences the effective dielectric felt by the bound electron−hole pair.

Dielectric Screening. We observe that exciton binding energies will increase with decreasing NPL thicknesses. To demonstrate this independent of our Elliott fits, we model the excitonic interactions in the NPL with an electron and a hole as point charges within a dielectric slab modeled after the dielectric constant of the NPL's ($\varepsilon_{NPL} \approx 10$). This region is sandwiched by an external dielectric equal to that of organic ligand environment ($\varepsilon_{ext} \approx 2$), illustrated in Figure 3a. We utilize the method of images to determine the excitonic electrostatic potential at one of the charges:[42]

https://doi.org/10.1021/acs.jpclett.1c00624
J. Phys. Chem. Lett. 2021, 12, 4958−4964

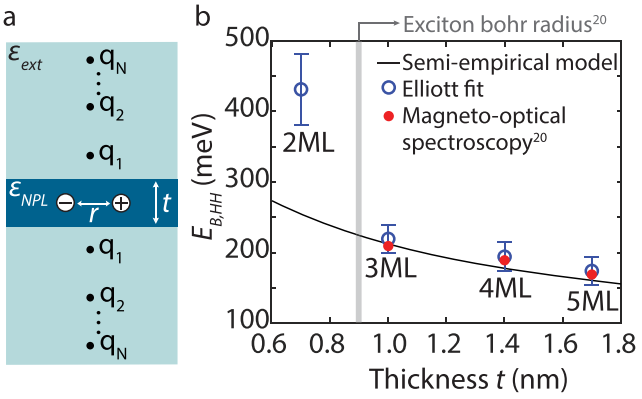

Figure 3. (a) Visualization of the exciton in the colloidal NPL system as represented in the method of images. (b) Relationship between exciton binding energy and CdSe NPL thickness, indicating the predicted trend of our semiempirical electrostatic model, extracted values from absorption spectra using the modified Elliott model, and measured values from magneto-optical spectroscopy.

$$V = \frac{q}{4\pi\varepsilon_0\varepsilon_{\mathrm{NPL}} r} + 2\sum_{N=1}^{\infty}\left[\left(\frac{\varepsilon_{\mathrm{NPL}} - \varepsilon_{\mathrm{ext}}}{\varepsilon_{\mathrm{NPL}} + \varepsilon_{\mathrm{ext}}}\right)^n \frac{q}{4\pi\varepsilon_0\varepsilon_{\mathrm{NPL}}\sqrt{r^2 + n^2t^2}}\right] \quad (3)$$

where q is the magnitude of the point charge, ε_0 is the vacuum permittivity, $\varepsilon_{\mathrm{NPL}}$ is the dielectric (i.e., relative permittivity) of the NPL, $\varepsilon_{\mathrm{ext}}$ is the effective dielectric of the external environment, r is the exciton Bohr radius, t is the NPL thickness, and N is the number of image charges (Figure 3a). The derivation of this potential equation and the effect of n on the extracted binding energy is explored in Supporting Informatin Section VI, where we show $N = 20$ image charges reproduce the full potential.

We equate this potential in eq 3 to an effective two-point charge Coulombic potential, V_{eff}, with an overall effective relative dielectric constant, $\varepsilon_{\mathrm{eff}}$:

$$V_{\mathrm{eff}} = \frac{q}{4\pi\varepsilon_0\varepsilon_{\mathrm{eff}} r} \quad (4)$$

Solving for $\varepsilon_{\mathrm{eff}}$ allows us to determine the exciton binding energy through the Rydberg equation:

$$E_{\mathrm{B}} = \frac{e^2}{8\pi\varepsilon_0^{\,2}\varepsilon_{\mathrm{eff}}^{\,2} r} \quad (5)$$

The Bohr radii values are derived from the diamagnetic shift coefficient (σ) obtained by magneto-optical spectroscopy performed by Brumberg et al. for 3−5 ML CdSe NPLs.[20] The E_{B} values for CdSe NPLs of varying thicknesses are shown in Figure 3b, where the data show good agreement to the trend line produced by taking the average σ and its corresponding E_{B}'s. In Supporting Information Section VI-C Figure S6, we describe in detail how each parameter is used to determine the continuous line plotted in Figure 3b. The electrostatic model captures the trend of decreasing E_{B} with thickness t, consistent with our Elliott fit and literature values of E_{B} for 3−5 ML CdSe NPLs, as shown in Table 1.

It should be noted that we represent electrostatic interactions through mean-field dielectric mediated Coulombic potential. Prior work in TMDCs has shown that the internal polarizability can be heavily dependent on the momentum direction.[43] We hypothesize this may be in part responsible for deviations of experiment to model particularly in thinner nanoplatelets, where the thickness of the NPLs is larger than the exciton Bohr radius (Figure 3b: gray line).[20] Our local effective potential computed from the method of images (eq 3) thus can be thought of as a first-order correction to the 3D binding energy equation. Indeed, in the Supporting Information Section VII, we compute the binding energy using a basis of hydrogenic orbitals for which we tune the coefficients variationally with the dielectric slab potential, which we find excellent agreement to our electrostatic model, but equivalent deviations for 2 ML NPLs. Our results suggest that future simulations of NPL excitons (including high-level GW and Bethe−Saltpeter methods) should consider the more complex termination of organic ligands to fully capture NPL binding energies, especially in quantum confined regimes.[44,45]

Controlling Exciton Binding Energy by Modulating External Dielectric. To confirm the extent to which external dielectric contrast modulates exciton binding energy, we change the solvent environment, similar to previous work in TMDCs and 2D perovskites.[28,46,47] We measure E_{B} and E_{G} using the above Elliott model fit of the absorption spectrum of 3 ML HgTe NPLs (Figure 4a-1), initially suspended in hexanes ($\varepsilon_{\mathrm{Hexanes}} \approx 1.9$). Then, acetonitrile (also known as MeCN, $\varepsilon_{\mathrm{MeCN}} \approx 38$) is added to the hexane layer, and the solutions are vortexed for 1 min. After letting it settle, the hexane layer is taken out and its

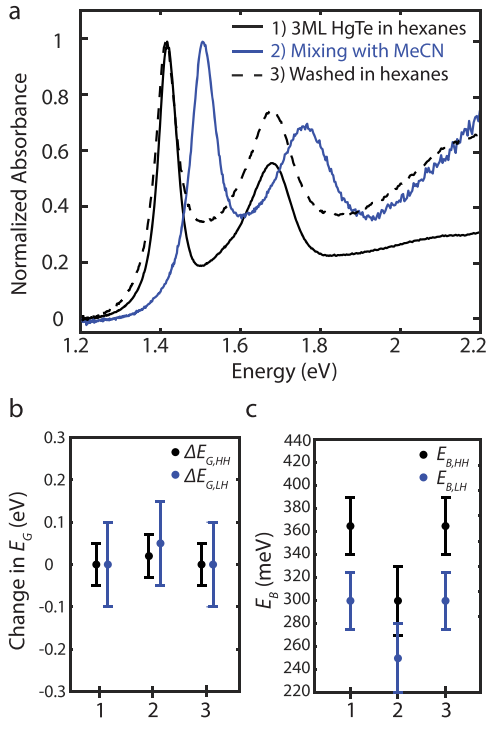

Figure 4. (a) Shift in the $X_{1,\mathrm{HH}}$ transition peak as 3 ML HgTe NPLs are vortexed with the MeCN mixture and then washed back into hexanes. The baseline increases due to increased Rayleigh scatter. (b) Minimal change in bandgap energy as it corresponds to (1) suspension in hexanes, (2) mixing with MeCN, and (3) washing in hexanes steps, as indicated in (a). (c) Exciton binding energy as it corresponds to steps 1−3, showing a significant decrease in E_{B} with constant E_{G} as the NPLs experience a higher solvent dielectric in step 2.

https://doi.org/10.1021/acs.jpclett.1c00624
J. Phys. Chem. Lett. 2021, 12, 4958−4964

absorption spectrum is measured (Figure 4a-2; the exact procedure can be found in Supporting Information Section VIII-A with FTIR in Figure S7, showing no sign of ligand exchange). Finally, the NPLs are returned to their initial hexane environment, after thoroughly washing away the MeCN, and we observe the recovery of the exciton absorption peak, but with increased Rayleigh scatter baseline (Figure 4a-3). Altogether, Figure 4a shows the resultant shift and recovery of the $X_{1,HH}$ peak of the HgTe spectrum as the NPLs are exposed to a higher dielectric environment and returned to hexanes. Panels b and c of Figure 4 demonstrate corresponding Elliott fit values that indicate an unchanged E_G in comparison to a 65 meV decrease in $E_{B,HH}$ and a 50 meV decrease in $E_{B,LH}$, supporting the hypothesis that we have increased the effective dielectric and thus lowered the E_B without changing the structure of the NPL. From the decreasing E_B's, we calculate a modest corresponding increase in ε_{eff} from 13.8 to 15.1, due to the MeCN (eq 5). Using eq 3, we can infer the increase in ε_{ext} from 2.0 to 3.3; this is notable as the dielectric of MeCN is 38. The small change in ε_{ext} suggests the continued dominance of the aliphatic ligands on the dielectric environment, meaning MeCN only has limited access to the excitonic field lines. Therefore, the shift in HgTe E_B can be attributed to the change in the effective dielectric—suggesting more significant impact of the external dielectric on NPL excitonic behavior, than previously recognized. However, we note that this procedure did not appear to alter the binding energy in cadmium selenide/telluride and mercury selenide nanocrystals (Supporting Information Section VII-C; Figures S8−S11), which we attribute to denser ligand coverage in these metal chalcogenide nanocrystals.[10]

Our results deviate from the known behaviors of 2D TDMC semiconductors, where the modification of the external dielectric is expected to change not only the exciton binding energy but also the bandgap. In the case of single-layer $MoSe_2$, the bandgap and binding energies both differed in comparing vacuum to bilayer graphene.[48,49] Raja et al. reported similar effects in monolayer WS_2, which showed micron-sized, spatial fluctuations of the external dielectric screening.[50] Interestingly, they observed minimal shifts in the $n = 1$ exciton peak, due to compensating shifts in the bandgap and exciton binding energy. However, we believe these complementary shifts in E_B and E_G are monolayer TMDC properties, and not a general feature of 2D semiconductors. In fact, Passarelli et al. demonstrated that the exciton binding energy in 2D perovskites can be tuned by doping the organic layer.[28] Here, they report an unchanged bandgap energy as they modulate the external dielectric by increasing the dopant concentration, while observing a decrease in the exciton binding energy. In general, we hypothesize that the effect of external dielectric will be more strongly felt in exciton binding energies and less so in bandgaps due to their relatively large Bohr radius.

Another consideration is that external dielectrics modify not only the strength of the exciton binding energy but also the spacing of the Rydberg levels. This effect is modeled by Olsen et al. with a modified Rytova−Keldysh formalism and observed in monolayer WS_2 by Chernikov et al.[45,51−56] In our work, a 3D Wannier exciton model shows good agreement to experimental data, and we lack the resolution to probe deviations from the classical Rydberg series. However, such deviations may also contribute to the apparent large binding energy observed in 2 ML platelets. We explored both a variational and perturbative treatment of the excitonic Hamiltonian (Supporting Information Section VII) and found results in good agreement with our effective dielectric model. However, there was no significant improvement in the apparent discrepancy observed for 2 ML platelets, suggesting the insufficiency of effective potential in describing binding energies in this limit.

Exciton binding energies are important experimental parameters that govern absorption, emission, and energy and charge transport. Using a modified Elliott model, we extract binding energies for many NPLs—several of them for the first time—that also show excellent agreement with prior limited measurements. This model represents a simple and accessible tool to probe excitonic and continuum transitions from absorption measurements, complementing sophisticated techniques such as magneto-optical spectroscopy or opto-acoustic methods, which were previously used.[20,57]

We also explore the effect of dielectric screening on NPL excitons using a simple semiempirical electrostatic model, which produced calculated E_B's that are in excellent agreement with measured binding energies for 3−5 ML CdSe NPLs. The model confirmed that unlike their bulk and 0D counterparts, nanoplatelet excitonic electrostatic field lines extend beyond the semiconductor itself and are modulated by the external environment. We experimentally confirm the effect of dielectric confinement by modifying NPL external environment and show a noticeable shift in exciton binding energy, consistent with similar measurements in 2D TMDCs and perovskites.[28,46,52] Uncovering the exciton binding energies of NPLs and understanding how external dielectric screening modulates these resonances further establishes the distinct properties of nanoplatelets that distinguish them from their quantum dot counterparts.

■ ASSOCIATED CONTENT

Supporting Information

The Supporting Information is available free of charge at https://pubs.acs.org/doi/10.1021/acs.jpclett.1c00624.

Materials, syntheses, characterization, table of EDS data, FTIR spectra, TEM images, fitting of absorption spectra, convolution steps for linewidth broadening, derivation of Elliott's formula, exciton binding energies, effect of Elliott model fitting, useful approximations, application of images method, table of binding energies, calculation steps of the exciton binding energy, diagram showing the calculation steps for the exciton binding energy, variational approach to binding energies, solvent washing, absorption spectra, and Elliott fit contributions (PDF)

■ AUTHOR INFORMATION

Corresponding Authors

Timothy L. Atallah − *Department of Chemistry and Biochemistry, University of California, Los Angeles, Los Angeles, California 90095-1569, United States*; Email: atallaht@denison.edu

Justin R. Caram − *Department of Chemistry and Biochemistry, University of California, Los Angeles, Los Angeles, California 90095-1569, United States*; orcid.org/0000-0001-5126-3829; Email: jcaram@chem.ucla.edu

https://doi.org/10.1021/acs.jpclett.1c00624
J. Phys. Chem. Lett. 2021, 12, 4958−4964

Authors

Ashley J. Shin − *Department of Chemistry and Biochemistry, University of California, Los Angeles, Los Angeles, California 90095-1569, United States;* orcid.org/0000-0001-8871-5753

Azmain A. Hossain − *Department of Chemistry and Biochemistry, University of California, Los Angeles, Los Angeles, California 90095-1569, United States*

Stephanie M. Tenney − *Department of Chemistry and Biochemistry, University of California, Los Angeles, Los Angeles, California 90095-1569, United States*

Xuanheng Tan − *Department of Chemistry and Biochemistry, University of California, Los Angeles, Los Angeles, California 90095-1569, United States*

Lauren A. Tan − *Department of Chemistry and Biochemistry, University of California, Los Angeles, Los Angeles, California 90095-1569, United States*

Jonathan J. Foley IV − *Department of Chemistry, William Paterson University, Wayne, New Jersey 07470, United States;* orcid.org/0000-0001-8814-4444

Complete contact information is available at: https://pubs.acs.org/10.1021/acs.jpclett.1c00624

Notes

The authors declare no competing financial interest.

■ ACKNOWLEDGMENTS

This work received partial support was given by National Science Foundation under Career Grant 1905242. Support was also given by the US Department of Energy, Office of Science, Basic Energy Sciences, under QI grant Award DE-SC0019245. A.A.H. acknowledges the Dolores C. Southam Summer Undergraduate Research Fellowship from the UCLA Department of Chemistry and Biochemistry. J.J.F. acknowledges support from the ART program at William Paterson University and the Research Corporation for Scientific Advancement Cottrell Scholar Award for support.

■ REFERENCES

(1) Tessier, M. D.; Mahler, B.; Nadal, B.; Heuclin, H.; Pedetti, S.; Dubertret, B. Spectrsocopy of Colloidal Semiconductor Core/shell Nanoplatelets with High Quantum Yield. *Nano Lett.* **2013**, *13*, 3321−3328.

(2) Nasilowski, M.; Mahler, B.; Lhuillier, E.; Ithurria, S.; Dubertret, B. Two-Dimensional Colloidal Nanoscrystals. *Chem. Rev.* **2016**, *116*, 10934−10982.

(3) Guzelturk, B.; Kelestemur, Y.; Olutas, M.; Delikanli, S.; Demir, H. V. Amplified Spontaneous Emission and Lasing in Colloidal Nanoplatelets. *ACS Nano* **2014**, *8*, 6599−6605.

(4) Grim, J. Q.; Christodoulou, S.; Di Stasio, F.; Krahne, R.; Cingolani, R.; Manna, L.; Moreels, I. Continuous-Wave Biexciton Lasing at Room Temperature Using Solution-Processed Quantum Wells. *Nat. Nanotechnol.* **2014**, *9*, 891−895.

(5) Ithurria, S.; Dubertret, B. Quasi 2d Colloidal Cdse Platelets With Thickness Controlled at the Atomic Level. *J. Am. Chem. Soc.* **2008**, *130*, 16504−16505.

(6) Bouet, C.; Mahler, B.; Nadal, B.; Abecassis, B.; Tessier, M. D.; Ithurria, S.; Xu, X.; Dubertret, B. Two-dimensional growth of CdSe nanocrystals from nanoplatelets to nanosheets. *Chem. Mater.* **2013**, *25*, 639−645.

(7) Izquierdo, E.; Dufour, M.; Chu, A.; Livache, C.; Martinez, B.; Amelot, D.; Patriarche, G.; Lequeux, N.; Lhuillier, E.; Ithurria, S. Coupled Hgse Colloidal Quantum Wells Through A Tunable Barrier: A Strategy To Uncouple Optical And Transport Band Gap. *Chem. Mater.* **2018**, *30*, 4065−4072.

(8) Meerbach, C.; Wu, C.; Erwin, S. C.; Dang, Z.; Prudnikau, A.; Lesnyak, V. Halide-Assisted Synthesis Of Cadmium Chalcogenide Nanoplatelets. *Chem. Mater.* **2020**, *32*, 566−574.

(9) Moghaddam, N.; Dabard, C.; Dufour, M.; Po, H.; Xu, X.; Pons, T.; Lhuillier, E.; Ithurria, S. Surface Modification Of Cde (E: S, Se, And Te) Nanoplatelets To Reach Thicker Nanoplatelets And Homostructures With Confinement-Induced Intraparticle Type I Energy Level Alignment. *J. Am. Chem. Soc.* **2021**, *143*, 1863−1872.

(10) Tenney, S. M.; Vilchez, V.; Sonnleitner, M. L.; Huang, C.; Friedman, H. C.; Shin, A. J.; Atallah, T. L.; Deshmukh, A. P.; Ithurria, S.; Caram, J. R. Mercury Chalcogenide Nanoplatelet-Quantum Dot Heterostructures as a New Class of Continuously Tunable Bright Shortwave Infrared Emitters. *J. Phys. Chem. Lett.* **2020**, *11*, 3473−3480.

(11) Hines, M. A.; Guyot-Sionnest, P. Synthesis and Characterization of Strongly Luminescing Zns-Capped Cdse Nanocrystals. *J. Phys. Chem.* **1996**, *100*, 468−471.

(12) Mahler, B.; Nadal, B.; Bouet, C.; Patriarche, G.; Dubertret, B. Core/Shell Colloidal Semiconductor Nanoplatelets. *J. Am. Chem. Soc.* **2012**, *134*, 18591−18598.

(13) Christodoulou, S.; Climente, J. I.; Planelles, J.; Brescia, R.; Prato, M.; Martin-Garcia, B.; Khan, A. H.; Moreels, I. Chloride-Induced Thickness Control in Cdse Nanoplatelets. *Nano Lett.* **2018**, *18*, 6248−6254.

(14) Ithurria, S.; Bousquet, G.; Dubertret, B. Continuous Transition from 3D to 1D Confinement Observed During the Formation of Cdse Nanoplatelets. *J. Am. Chem. Soc.* **2011**, *133*, 3070−3077.

(15) Sun, H.; Buhro, W. E. Core-shell cadmoim telluride quantum platelets with absorptions spanning the visible spectrum. *ACS Nano* **2019**, *13*, 6982−6991.

(16) Chaves, J.; Ribeiro, M.; Frederico, T.; Peres, N. M. R. Excitonic Effects in the Optical Properties of 2d Materials: An Equation of Motion Approach. *2D Mater.* **2017**, *4*, 025086.

(17) Van der Donck, M.; Peeters, F. M. Interlayer Excitons in Transition Metal Dichalcogenide Heterostructures. *Phys. Rev. B: Condens. Matter Mater. Phys.* **2018**, *98*, 115104.

(18) Wannier, H. The Structure of Electronic Excitation Levels in Insulating Crystals. *Phys. Rev.* **1937**, *52*, 191−197.

(19) Elliott, J. Intensity of Optical Absorption by Excitons. *Phys. Rev.* **1957**, *108*, 1384−1389.

(20) Brumberg, A.; Harvey, S. M.; Philbin, J. P.; Diroll, B. T.; Lee, B.; Crooker, S. A.; Wasielewski, M. R.; Rabani, E.; Schaller, R. D. Determination of the In-plane Exciton Radius in 2d Cdse Nanoplatelets via Magneto-Optical Spectrocopy. *ACS Nano* **2019**, *13*, 8589−8596.

(21) Scott, R.; Achstein, A. W.; Prudnikau, A. V.; Antanovich, A.; Siebbeles, L. D. A.; Artemyev, M.; Woggon, U. Time-Resolved Stark Spectroscopy in Cdse Nanoplatelets: Exciton Binding Energy, Polarizability, and Field-Dependent Radiative Rates. *Nano Lett.* **2016**, *16* (10), 6576−6583.

(22) Chhowalla, M.; Jena, D.; Zhang, H. Two-Dimensional Semiconducors for Transistors. *Nat. Rev. Mater.* **2016**, *1*, 16052.

(23) Christol, P.; Lefebvre, P.; Mathieu, H. A Single Equation Describes Excitonic Absorption Spectra in All Quantum-Sized Semiconductors. *IEEE J. Quantum Electron.* **1994**, *30*, 2287−2292.

(24) Green, M. A.; Ho-Baillie, A.; Snaith, H. J. The Emergence of Perovskite Solar Cells. *Nat. Photonics* **2014**, *8*, 506−514.

(25) Blakemore, S. Semiconducting and Other Major Properties of Gallium Arsenide. *J. Appl. Phys.* **1982**, *53*, R123.

(26) Feldmann, J.; Peter, G.; Gobel, E. O.; Dawson, P.; Moore, K.; Foxon, C.; Elliott, R. J. Linewidth Dependence of Radiative Exciton Lifetimes in Quantum Wells. *Phys. Rev. Lett.* **1988**, *60*, 243.

(27) Manser, J. S.; Christians, J. A.; Kamat, P. V. Intriguing Optoelectronic Properties of Metal Halide Perovskites. *Chem. Rev.* **2016**, *116*, 12956−13008.

(28) Passarelli, J. V.; Mauck, C. M.; Winslow, S. W.; Perkinson, C. F.; Bard, J. C.; Sai, H.; Williams, K. W. Tunable Exciton Binding Energy in 2d Hybrid Layered Perovskites through Donor-Acceptor

Interactions within the Organic Layer. *Nat. Chem.* **2020**, *12*, 672−682.
(29) Vasiliev, R. B.; Lebedev, A. I.; Lazareva, E. P.; Shlenskaya, N. N.; Zaytsev, V. B.; Yao, A. G.; Vitukhnovsky, Y.; Sakoda, K. High-Energy Exciton Transitions in Quasi Two-Dimensional Cadmium Chalcogenide Nanoplatelets. *Phys. Rev. B: Condens. Matter Mater. Phys.* **2017**, *95*, 165414.
(30) Moghaddam, N.; Greboval, C.; Qu, J.; Chu, A.; Rastogi, P.; Livache, C.; Khalili, A.; Xu, X. Z.; Baptiste, B.; Klotz, S.; Fishman, G.; Capitani, F.; Ithurria, S.; Sauvage, S.; Lhuillier, E. The Strong Confinement Regime in HgTe Two-Dimensional Nanoplatelets. *J. Phys. Chem. C* **2020**, *124*, 23460−23468.
(31) Fernandez, M.; Prete, P.; Lovergine, N.; Mancini, A. M.; Cingolani, R.; Vasanelli, L.; Perrone, M. R. Optical Properties of MOVPE-grown ZnS Epilayers on (100)GaAs. *Phys. Rev. B: Condens. Matter Mater. Phys.* **1997**, *55*, 7660−7666.
(32) Campi, D.; Coriasso, C. Optical Nonlinearities in Multiple Quantum Wells: Generalized Elliott Formula. *Phys. Rev. B: Condens. Matter Mater. Phys.* **1995**, *51*, 10719−10728.
(33) Soloviev, V. N.; Eichhofer, A.; Fenske, D.; Banin, U. Molecular Limit of a Bulk Semiconductor: Size Dependence of the "Band Gap" in CdSe Cluster Molecules. *J. Am. Chem. Soc.* **2000**, *122*, 2673−2674.
(34) Warlimont, H.; Martienssen, W. *Springer Handbook of Materials Data*; Springer, 2018.
(35) Kumar, M. M. D.; Devadason, S. Structural and Optical Properties Of CdTe/CdSe Heterostructure Multilayer Thin Films Prepared by Physical Vapor Deposition Technique. *Appl. Nanosci.* **2013**, *3*, 453−459.
(36) Akinlami, J. O.; Odeyemi, O. O. Electronic Structure and Optical Properties of HgSe. *Fiz. Napivprovidn., Kvantova Optoelektron.* **2018**, *21*, 288−293.
(37) Livache, C.; Goubet, N.; Greboval, C.; Martinez, B.; Ramade, J.; Qu, J.; Triboulin, A.; Cruguel, H.; Baptiste, B.; Klotz, S.; et al. Effect of Pressure on Interband and Intraband Transition of Mercury Chalcogenides Quantum Dots. *J. Phys. Chem. C* **2019**, *123*, 13122−13130.
(38) Baars, J.; Sorger, F. Reststrahlen Spectra of HgTe and CdxHg1-xTe. *Solid State Commun.* **1972**, *10*, 875−878.
(39) Geick, R.; Perry, C. H.; Mitra, S. S. Lattice Vibrational Properties of Hexagonal CdSe. *J. Appl. Phys.* **1966**, *37*, 1994−1997.
(40) He, K.; Poole, C.; Mak, K. F.; Shan, J. Experimental Demonstration of Continuous Electronic Structure Tuning via Strain in Atomically Thin MoS2. *Nano Lett.* **2013**, *13*, 2931−2936.
(41) Peelaers, H.; de Walle, C. G. V. Effects of Strain on Band Structure and Effective Masses in Mos2. *Phys. Rev. B: Condens. Matter Mater. Phys.* **2012**, *86*, 241401.
(42) Jackson, J. D. *Classical Electrodynamics*, 3rd ed.; Wiley, 1998.
(43) Cudazzo, P.; Attaccalite, C.; Tokatly, I. V.; Rubio, A. Strong Charge-Transfer Excitonic Effects and the Bose−Einstein Exciton Condensate in Graphane. *Phys. Rev. Lett.* **2010**, *104*, 226804.
(44) Greenwood, A. R.; Mazzotti, S.; Norris, D. J.; Galli, G. Determining the Structure—Property Relationships of Quasi-Two-Dimensional Semiconductor Nanoplatelets. *J. Phys. Chem. C* **2021**, *125*, 4820−4827.
(45) Olsen, T.; Latini, S.; Rasmussen, F.; Thygesen, K. S. Simple Screened Hydrogen Model of Excitons in Two-Dimensional Materials. *Phys. Rev. Lett.* **2016**, *116*, 056401.
(46) Lin, Y.; Ling, X.; Yu, K.; Huang, S.; Hsu, A. L.; Lee, Y. H.; Kong, J.; Dresselhaus, M. S.; Palacios, T. Dielectric Screening of Excitons and Trions in Single-layer MoS2. *Nano Lett.* **2014**, *14*, 5569−5576.
(47) Choi, J.; Zhang, H.; Du, H.; Choi, J. H. Understanding Solvent Effects on the Properties of Two-Dimensional Transition Metal Dichalcogenides. *ACS Appl. Mater. Interfaces* **2016**, *8*, 8864−8869.
(48) Ugeda, M. M.; Bradley, A. J.; Shi, S.; da Jornada, F. H.; Zhang, Y.; Qiu, D. Y.; Ruan, W.; Mo, S. K.; Hussain, Z.; Shen, Z.; Wang, F.; Louie, S. G.; Crommie, M. F. Giant Bandgap Renormalization and Excitonic Effects in a Monolayer Transition Metal Dichalcogenide Semiconductor. *Nat. Mater.* **2014**, *13*, 1091−1095.
(49) Thygesen, K. S. Calculating Excitons, Plasmons, and Quasiparticles in 2D Materials and van der Waals Heterostructures. *2D Mater.* **2017**, *4*, 022004.
(50) Raja, A.; Waldecker, L.; Zipfel, J.; Cho, Y.; Brem, S.; Ziegler, J. D.; Kulig, M.; Taniguchi, T.; Watanabe, K.; Malic, E.; Heinz, T. F.; Berkelbach, T. C.; Chernikov, A. Dielectric Disorder in Two-Dimensional Materials. *Nat. Nanotechnol.* **2019**, *14*, 832−837.
(51) Chernikov, A.; Berkelbach, T. C.; Hill, H. M.; Rigosi, A.; Li, Y.; Aslan, O. B.; Reichman, D. R.; Hybertse, M. S.; Heinz, T. F. Exciton Binding Energy and Nonhydrogenic Ryberg Series in Monolayer WS_2. *Phys. Rev. Lett.* **2014**, *113*, 076802.
(52) Rytova, N. S. Screened Potential of a Point Charge in a Thin Film. *Mosc. Univ. Phys. Bull.* **1967**, *22*, 18.
(53) Keldysh, L. V. Coulomb Interaction in Thin Semicondcutor and Semimetal Films. *JETP Lett.* **1979**, *29*, 658−660.
(54) Cavalcante, L. S. R.; Chaves, A.; Duppen, V.; Peeters, F. M.; Reichman, D. R. Electrostatics of Electron-hole Interactions in van der Waals Heterostructures. *Phys. Rev. B: Condens. Matter Mater. Phys.* **2018**, *97*, 125427.
(55) Latini, S.; Olsen, T.; Thygesen, K. S. Excitons in van der Waals Heterostructures: The Important Role of Dielectric Screening. *Phys. Rev. B: Condens. Matter Mater. Phys.* **2015**, *92*, 245123.
(56) Cudazzo, P.; Tokatlly, I. V.; Rubio, A. Dielectric Screening in Two-Dimensional Insulators: Implications of Excitonic and Impurity States in Graphane. *Phys. Rev. B: Condens. Matter Mater. Phys.* **2011**, *84*, 085406.
(57) Zelewski, S. J.; Nawrot, K. C.; Zak, A.; Gladysiewicz, M.; Nyk, M.; Kudrawiec, R. Exciton Binding Energy of Two-dimensional Highly Luminescent Colloidal Nanostructures Determine from Combined Optical and Photoacoustic Spectroscopies. *J. Phys. Chem. Lett.* **2019**, *10*, 3459−3464.

https://doi.org/10.1021/acs.jpclett.1c00624
J. Phys. Chem. Lett. 2021, 12, 4958−4964